ZINC-AIR MICROBATTERY WITH ELECTRODE ARRAY OF ZINC MICROPOSTS

Fardad Chamran[1], Hong-Seok Min[2], Bruce Dunn[2] and Chang-Jin "CJ" Kim[1]
[1]Mechanical and Aerospace Engineering Dept., [2]Materials Science and Engineering Dept.
University of California, Los Angeles (UCLA), U.S.A.

ABSTRACT

We report the first successful development of a high performance MEMS-fabricated zinc-air microbattery. The key feature of this battery is the 3-dimensional architecture of the zinc electrode, which consists of an array of high aspect ratio microposts. This design efficiently increases the surface area of the zinc electrode and improves the performance of the battery at high discharge rates. The superior performance over commercially available batteries is demonstrated through high discharge rate tests as well as powering a real device. A surface-mounted LED was integrated into the microbattery package as the device, and the illumination of the LED was monitored during the discharge.

INTRODUCTION

Three-dimensional (3D) battery architectures have been proposed as a new direction in miniaturizing portable power sources [1]. These architectures are based on developing 3D electrode arrays of high-aspect-ratio microposts. The post-array configuration makes use of the out-of-plane dimension in contrast to traditional thin-film battery electrodes, which are 2D and use only the in-plane surface.

Using a post-array configuration for the electrodes, we previously introduced a 3D nickel-zinc microbattery [2] and a carbon post electrode for lithium-ion battery [3]. Different types of 3D architectures, such as nano-scale aerogel electrodes and micron size post electrodes have been recently reviewed [4]. 3D electrodes consisting of micro post-arrays have already demonstrated some of these improvements for lithium-ion half-cell systems [5,6]. A sandwich-like thin-film battery structure has also been formed in a perforated substrate to demonstrate a 3D lithium-ion battery [7].

In this paper, we have focused on the primary zinc-air system due to its high energy density. Zinc-air battery consists of zinc anode, air (oxygen) cathode and an alkaline (e.g. potassium hydroxide) electrolyte. Since the cathode material is oxygen, it can be provided from the ambient air. This leads to high energy densities, resulting from the increased volume available for the zinc anode. The cathode electrode acts only as a reaction site to reduce the oxygen and is not consumed. The main characteristic of the post-array zinc-air architecture is the high discharge rate capabilities, which may not exist for the commercially available zinc-air cells. The advantage of this design is discussed in this paper, as well as its high discharge rate performance during discharge tests and powering of a device.

DESIGN

In today's technology, zinc-air battery is primarily fabricated in the form of button cells with applications in hearing aid devices [8]. The anode is in the form of a zinc powder mixed with a gelling agent. Although the active surface area of the zinc powder electrode is high, the battery cannot access its high energy at high discharge rates because zinc oxide is formed on the powder surface and results in high internal resistance. To alleviate this problem, we propose post-array zinc electrode architecture. In this configuration, the zinc anode is made out of an array of high aspect ratio microposts on top of a nickel current collector (Fig. 1). During the discharge, the zinc posts get gradually oxidized on the surface but the internal resistance is still kept low due to the zinc core of the posts. The electrons generated reach the current collector through the zinc core of the posts, without having to go though the zinc oxide. This prevents ohmic losses during discharge, and the battery can function efficiently at high discharge rates.

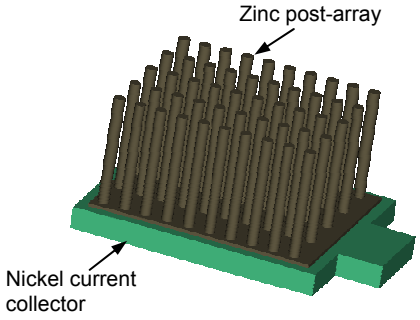

Fig. 1 Schematic of Zinc post-array electrode

FABRICATION

Fig. 2 schematically depicts the fabrication process. In step 1, the silicon mold featuring an array of dense holes is fabricated. To achieve high aspect ratio holes, n-type silicon was anodically etched in HF during backside illumination [9]. It was etched at 4 V bias in 4 % HF. The current density was kept constant at 6 mA/cm^2 by adjusting the illumination intensity. 1000 Å of thermal-

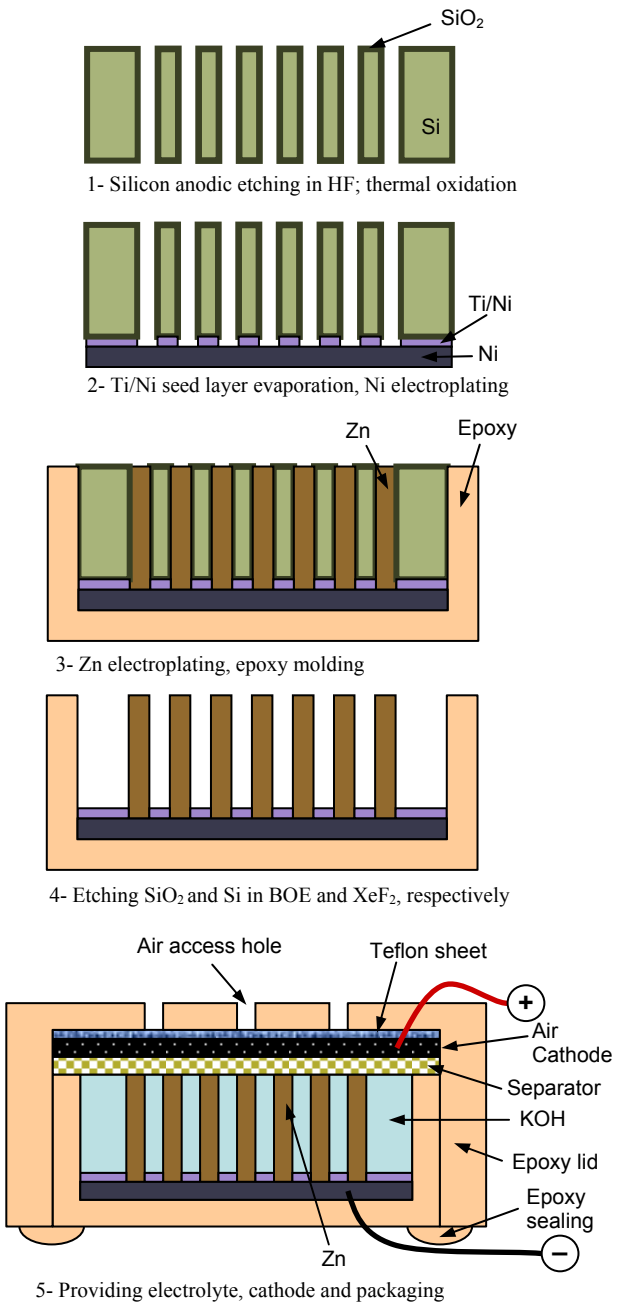

Fig. 2 Fabrication process of zinc-air microbattery with zinc post-array electrode

oxide was grown to passivate the silicon for the following metallization steps. In step 2, a Ti/Ni (100/1000 Å) seed layer was evaporated, and a 20 µm nickel current collector was electroplated at the bottom surface to close the open holes. Nickel was electroplated at constant current density of 10 mA/cm^2 using commercial nickel electroplating solution (Technic Inc.) In step 3, zinc was electroplated in the high aspect ratio holes. The zinc electroplating solution was prepared by dissolving zinc sulfate (240 g), ammonium chloride (15 g), aluminum sulfate (30 g) and saccharin (1 g) in one liter of deionized (DI) water [10]. Nickel current collector was used as the electroplating seed layer during this step. Zinc was electroplated at constant current density of 20 mA/cm^2. A tape protected the nickel layer from being electroplated with zinc. In step 3, the housing of the battery was provided by molding the sample in epoxy. In step 4, silicon and silicon dioxide were etched in XeF_2 and BOE, respectively. In step 5, the zinc anode was assembled with the other components of the battery. The air cathode was commercially available (Duracell) and consisted of carbon and a small amount of manganese dioxide catalyst. The air cathode was laminated with a porous separator on one side and a porous Teflon sheet on the other side. The separator acts as the ionic conductor between the electrodes and as an insulator to prevent internal short-circuiting. The Teflon layer allows oxygen to diffuse into the cell and also seals the battery from leaking the electrolyte. 6 M aqueous solution of potassium hydroxide (KOH) was used as the electrolyte. The battery was packaged using an epoxy lid. The air access holes were provided on the lid during the molding step. The lid and the bottom housing were sealed using epoxy glue at the interfaces. Fig. 3 is an SEM image of zinc post-array prior to assembly with other components. The location of the missing posts was chosen to show the entire height of the posts. The posts are 10 µm in diameter and 200 µm tall.

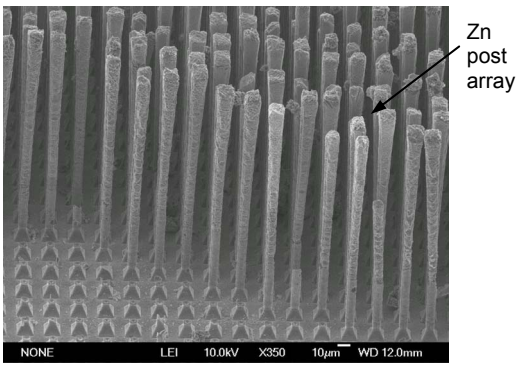

Fig. 3 SEM image of zinc post-array

EXPERIMENTAL

A. Discharge Tests

The fabricated batteries were tested under different discharge rates. Fig. 4 is the galvanostatic discharge curve of a sample at 3.3 mA/cm^2. The voltage has maintained a constant value of 1.25 V during the discharge period. The battery components were dissembled after testing and the morphology of the zinc post-array structure was observed. Fig. 5 is the SEM image of a post-array electrode after the discharge test. Although the posts are distorted due to uneven stress distribution during the test, they are still attached to the nickel current collector and functional. All of the zinc posts are turned into hollow zinc oxide posts after the complete discharge. The formation of this hollow structure can be explained by the Kirkendall effect, which

is due to differential diffusion rates of the reactants in Zn dissolution-precipitation reaction [11]. The hollow ZnO formation shows that the zinc posts are gradually oxidized from the surface and supports the functionality of post-array electrode architectures.

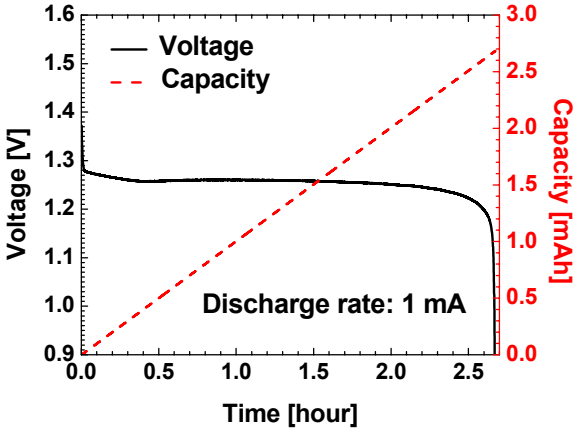

Fig. 4 Discharge characteristics of zinc-air microbattery with post-array electrode

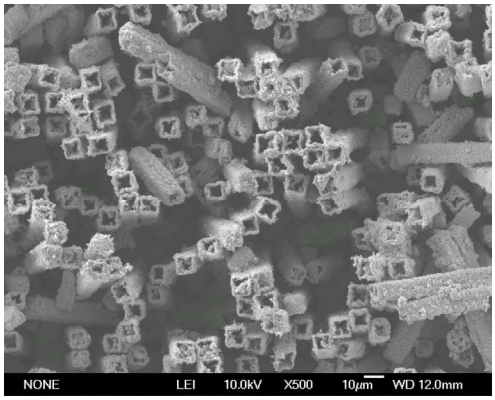

Fig. 5 SEM image of zinc post-array electrode after the discharge test

The performance of this battery at high discharge rates is demonstrated and compared with that of the commercial batteries in Fig. 6. The batteries with post-array electrodes were fabricated in similar sizes as the commercial button zinc-air cells (Duracell DA10). Both types of the batteries were discharged at varying discharged rates. As can be seen in Fig. 6, the normalized energy density quickly drops for the commercial battery at high discharge rates, while the battery with post-array electrode maintains its high capacity even at high discharge rates. In this figure, the discharge rate is demonstrated using C-rate, which is defined as the discharge rate (mA) divided by the total capacity (mAh). The normalized energy density is the energy density divided by the calculated energy density. The post-array zinc-air batteries were tested in the current range from 0.1 mA to 5 mA.

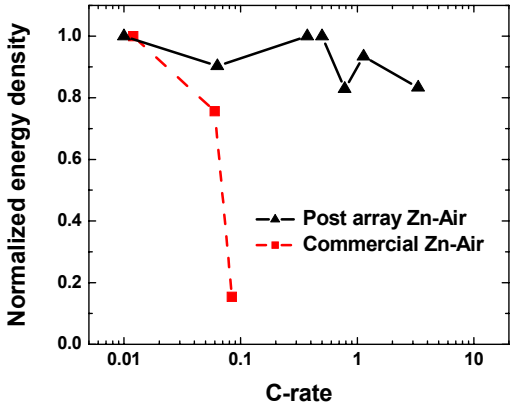

Fig. 6 Normalized energy density vs. C-rate for post-array and commercial zinc-air battery

B. Demonstration to Power an LED

The second part of our experiment was to assess the battery by powering a real device. The performance of the cell was compared with that of the commercial button cell during powering of a surface-mounted LED. To provide enough voltage to properly illuminate the LED, two zinc-air cells were connected in series. Fig. 7 shows the schematic of assembling the LED with the batteries. The two batteries and the LED were packaged by epoxy molding on top of each other to minimize the footprint area. The epoxy cover and electric connections are not shown. Fig. 8 is a picture captured during the illumination of the LED. The voltage and the current of the battery were monitored as depicted in the figure. To properly evaluate the performance against the commercial battery, the zinc powder was extracted from a commercial battery and placed in our epoxy housing. Fig. 9 shows the performance curve for the cell with post-array electrode during the LED illumination, along with that for the zinc powder cell in similar conditions. The voltage and the illumination intensity quickly dropped for powder cells due to increasing internal resistance, while the post-array electrode cells held a relatively flat voltage during the discharge as low resistance was maintained.

CONCLUSION

A micropost-array architecture for zinc electrodes of a primary (non-rechargeable) zinc-air battery was successfully designed, fabricated, and tested. The performance of the post-array zinc-air microbattery was investigated through galvanostatic discharge behavior. The investigation showed high discharge capability of the post-array zinc-air microbatteries. With the proven functionality, powering of an LED was demonstrated. Two post-array zinc-air microbatteries, placed in series,

successfully lit up the LED with enhanced performance over commercial zinc powder cells.

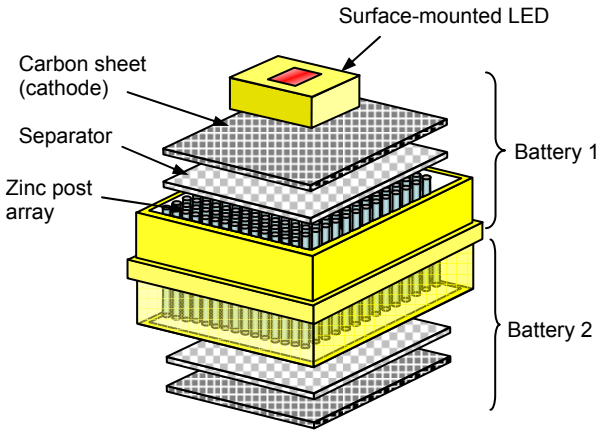

Fig. 7 Two microbatteries connected in series and packaged with an LED (connections not shown)

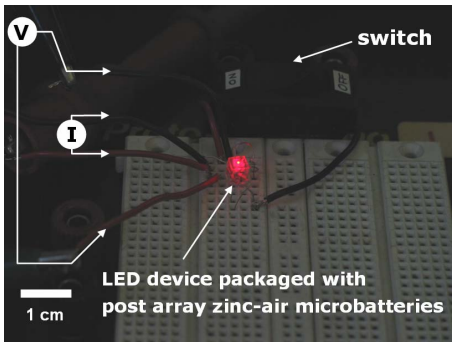

Fig. 8: LED illumination during testing. Voltage (V) and current (I) are measured during the test

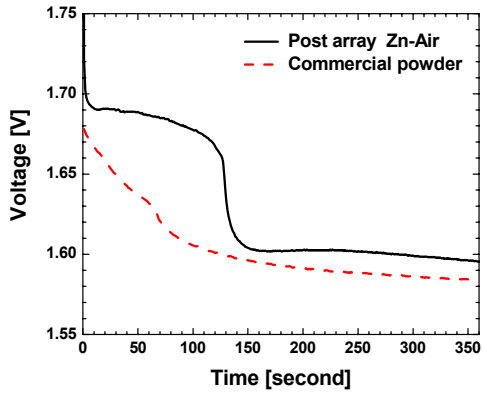

Fig. 9 Voltage curves of an LED, powered by post-array and commercial powder zinc-air microbatteries

ACKNOWLEDGMENTS

This work has been supported by the Office of Naval Research, through MURI grant N00014-01-1-0757.

REFERENCES

1. R. W. Hart, H. White, B. Dunn, and D. Rolison, "3-D Microbatteries", *Electrochemistry Communications*, **5** (2003), pp. 120-123.
2. F. Chamran, H.-S. Min, B. Dunn and C.-J. Kim, "Three-Dimensional Nickel-Zinc Microbatteries," Proc. IEEE Int. Conf. Micro Electro Mechanical Systems (MEMS'06), Istanbul, Turkey, Jan. 2006, pp. 950-953.
3. F. Chamran, U.-C. Yi and C.-J. Kim, "Metal-Cored Carbon Microposts for Three-Dimensional Li Ion Microbattery," Proc. Solid-State Sensors, Actuators and Microsystem Workshop (Hilton Head'06), Hilton Head Island, SC, USA, June 2006, pp. 185-188.
4. J. W. Long, B. Dunn, D. Rolison, and H. S. White, "Three-Dimensional Battery Architecture", *Chemical Reviews,* **104** (2004), pp. 4463-4492.
5. F. Chamran, Y. Yeh, B. Dunn and C.-J. Kim, "3-Dimensional Electrodes for Microbatteries", *Proc. ASME Int. Mechanical Eng. Congress*, Anaheim, CA, USA, Nov. 2004, IMECE2004-61925.
6. C. Wang, L.Taherabadi, G. Jia, M. Madou, Y. Yeh, and B. Dunn, "C-MEMS for the Manufacture of 3D Microbatteries", *Electrochemical and Solid State Letters*, **7** (2004), pp. A435-A438.
7. M. Nathan, D. Golodnitsky, V. Yufit, E. Strauss, T. Ripenbein, I. Shechtman, S. Menkin and E. Peled, "Recent Advances in Three Dimensional Thin Film Microbatteries", *Materials Research Society Symp.* Proc., **835** (2005), pp. K10.10.1- K10.10.6.
8. Colin A. Vincent and Bruno Scrosati, "Modern Batteries", Second Edition, John Wiley & Sons, Inc. (1997).
9. V. Lehmann and H. Foll, "Formation Mechanism and Properties of Electrochemically Etched Trenches in N-type Silicon," *J. Electrochemical Society*, **137** (1990), pp. 653-659.
10. F. A. Lowenheim, Modern Electroplating, Second ed. New York: Wiley, 1963.
11. K. N. Tu and U. Gosele, "Hollow Nanostructures Based on the Kirkendall Effect: Design and Stability Consideration," *Applied Physics Letters*, **86** (2005), pp. 093111-3.